Acoustic propulsion of a small, bottom-heavy sphere

François Nadal[1,†] **and Sébastien Michelin**[2]

[1]Wolfson School of Mechanical Electrical and Manufacturing Engineering, Loughborough University, Loughborough LE11 3TU, UK

[2]LadHyX – Département de Mécanique, CNRS – École Polytechnique, Institut Polytechnique de Paris, 91128 Palaiseau, France

We present here a comprehensive derivation for the speed of a small bottom-heavy sphere forced by a transverse acoustic field and thereby establish how density inhomogeneities may play a critical role in acoustic propulsion. The sphere is trapped at the pressure node of a standing wave whose wavelength is much larger than the sphere diameter. Due to its inhomogeneous density, the sphere oscillates in translation and rotation relative to the surrounding fluid. The perturbative flows induced by the sphere's rotation and translation are shown to generate a rectified inertial flow responsible for a net mean force on the sphere that is able to propel the particle within the zero-pressure plane. To avoid an explicit derivation of the streaming flow, the propulsion speed is computed exactly using a suitable version of the Lorentz reciprocal theorem. The propulsion speed is shown to scale as the inverse of the viscosity, the cube of the amplitude of the acoustic field and is a non-trivial function of the acoustic frequency. Interestingly, for some combinations of the constitutive parameters (fluid-to-solid density ratio, moment of inertia and centroid to centre of mass distance), the direction of propulsion is reversed as soon as the frequency of the forcing acoustic field becomes larger than a certain threshold. The results produced by the model are compatible with both the observed phenomenology and the orders of magnitude of the measured velocities.

Key words: propulsion, swimming/flying

---

1. Introduction

Controlled propulsion of microscopic objects in viscous flows has recently attracted much attention for its potential biomedical applications such as drug transport and delivery (Burdick *et al.* 2008; Sundararajan *et al.* 2008; Nelson, Kaliakastos & Abbott 2010) or analytical sensing in biological media (Campuzano *et al.* 2011; Wu *et al.* 2010). Self-propulsion in viscous flows requires temporal and spatial symmetry breaking (Purcell 1977; Lauga & Powers 2009). Based on that principle, many different mechanisms have been proposed to achieve propulsion of small rigid objects

† Email address for correspondence: F.R.Nadal@lboro.ac.uk

(see the reviews of Ebbens & Howse (2010), Wang *et al.* (2013)) and they generally belong to either of the two following categories.

The first and most classical group exploits an externally applied directional field, that effectively breaks the symmetry of the system at a scale much larger than the particle size, and drives the object in a specific direction. Electrophoresis (Smoluchowsky 1921) and diffusiophoresis (Anderson 1989) both fall in this first group, and result from the application of macroscopic electric or chemical gradients. The alternative approach relies on the local interaction of the particle with its close environment. Taking advantage of its own asymmetry, the particle converts locally the energy provided by a non-directional forcing field to break symmetry and self-propel.

For instance, catalytic bimetallic microrods can propel themselves (self-electro-phoresis) at high velocities (up to 10 μm s^{-1}) by oxidizing hydrogen peroxide and exploiting the resulting self-generated local electric fields (see e.g. Paxton *et al.* 2004, Ibele *et al.* 2007, Ebbens & Howse 2011). For non-ionic solutes, the concentration gradient can also trigger a net motion of the particle through self-diffusiophoresis (Pavlick *et al.* 2011, 2013; Golestanian, Liverpool & Ajdari 2007; Cordova-Figueroa & Brady 2008). Similarly, autonomous propulsion can be achieved by taking advantage of self-thermophoresis effects (Jiang, Yoshinaga & Sano 2010; Baraban *et al.* 2012; Qian *et al.* 2013). Unfortunately, electrochemically and thermally based methods are not biocompatible as a result of the inherent toxicity of the involved fuels (hydrogen peroxide, hydrazine) or of the required temperature differences.

Alternatively, acoustic fields may be used to achieve autonomous motion in biofluids, which explains the increasing interest of the scientific community in this type of propulsion method. Wang *et al.* (2012) demonstrated experimentally that bimetallic rods with asymmetric shape or composition were able to self-propel with velocities up to 200 μm s^{-1} when trapped in the nodal plane of an acoustic resonator. This pioneering work was soon extended to various configurations and geometries, and self-acoustophoresis of magnetic clusters or asymmetric particles was thus reported (Sabrina *et al.* 2018; Ahmed *et al.* 2014, 2016). Kaynak *et al.* (2017) showed that bioinspired acoustic microswimmers with dedicated shapes were even able to reach velocities up to 1200 μm s^{-1}. Although the prescribed acoustic field from which self-propulsion originates is directional, self-propulsion is achieved in a plane orthogonal to the excitation and its direction is not set by the external driving in contrast, for instance, with classical electrophoretic migrations of particles along the imposed forcing.

Since the seminal work of Wang *et al.* (2012), acoustic propulsion has been repeatedly ascribed to the streaming flows self-generated by the particle's periodic motion with respect to its fluid environment of small yet finite inertia (Riley 1966; Nadal & Lauga 2014; Collis *et al.* 2017; Kaynak *et al.* 2017). To analyse the potential role of a particle's asymmetric shape on its ability to self-propel, Nadal & Lauga (2014) first derived an integral form of the steady axial velocity of an acoustically forced near-sphere, exploiting the absence of rotation of the particle at leading order in the particle's asymmetry as suggested by Zhang & Stone (1998). Lippera *et al.* (2019) recently showed, however, that this configuration did not actually yield any propulsion at leading order and that higher-order corrections in the particle's asymmetry were necessary to obtain a rectified effect. Collis *et al.* (2017) considered the opposite case of an asymmetric (in density or shape) dumbbell of large aspect ratio, and showed that the propelling streaming flow actually arose from the inertial coupling between the viscous flows, respectively, generated by the particle's translation and rotation,
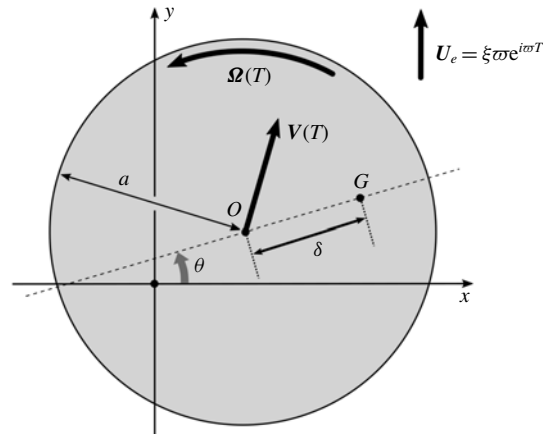
FIGURE 1. Oscillations of a bottom-heavy sphere forced by a uniform external oscillating flow. Here, ξ and ϖ are the displacement amplitude and frequency of the forcing acoustic field. The radius of the sphere is denoted by a, and δ refers to the centroid-to-centre of mass distance OG.

suggesting that acoustically generated rotation of the particle was just as essential as its periodic translation in order to obtain acoustic propulsion.

Inspired by this observation, we analyse here how acoustic self-propulsion of a geometrically symmetric particle (i.e. a sphere) may be achieved when its non-uniform density results in a combined translation and rotation under the effect of the acoustic forcing. We thus present the full analytical derivation of the leading-order propulsion velocity of a non-homogeneous sphere trapped at the nodal plane of a resonator. The centre of mass and centroid of the sphere do not coincide anymore, and as a result an inertial torque is imposed on the acoustically forced sphere driving a combination of translational and rotational motions. We demonstrate that spherical particles may thus self-propel thanks to a symmetry breaking in the hydrodynamic stress resulting from the inertial coupling of the viscous flows associated with the particle's combined translation and rotation, as suggested by Collis *et al.* (2017).

The paper is organized as follows. Section 2 is devoted to the derivation of the linear translational and rotational viscous responses of a non-homogeneous sphere to the transverse acoustic forcing. The leading-order inertial propulsion velocity of such a sphere is obtained in § 3 by means of a suitable version of the Lorentz reciprocal theorem. The physical relevance of this model to experimental observations is then discussed in § 4. Finally, our main findings are summarized in § 5.

2. Acoustically forced dynamics of a sphere in a viscous fluid

2.1. *Configuration and main assumptions*

We consider here the dynamics of a solid sphere of radius a and mean density ρ_s forced by a viscous periodic flow of density ρ and kinematic viscosity ν. The density distribution of the solid sphere is not homogeneous, so that the centre of mass G departs from its centroid O (figure 1). The mass and volume of the sphere are $m_s = \rho_s \mathcal{V}_s$ and $\mathcal{V}_s = (4/3)\pi a^3$, respectively.

The forcing (acoustic) flow $\boldsymbol{U}_e$ is uniform, harmonic of frequency ϖ and directed along the y-direction. This configuration corresponds to a sphere of size a trapped at

the pressure node of a standing acoustic wave of wave vector $\boldsymbol{k} = k\,\boldsymbol{e}_y$ in the limit $ka \ll 1$ (with $(\boldsymbol{e}_x, \boldsymbol{e}_y, \boldsymbol{e}_z)$ are the Cartesian unit vectors). In such a case, the incident flow can be considered as locally incompressible and to depend only on y. We consider in the following that the external forcing flow is uniform and takes the simple harmonic form

$$\boldsymbol{U}_e = \hat{\boldsymbol{U}}_e\,\mathrm{e}^{\mathrm{i}\varpi\,T} = \xi\varpi\,\mathrm{e}^{\mathrm{i}\varpi\,T}\,\boldsymbol{e}_y, \tag{2.1}$$

where ξ is the amplitude of the fluid particles' displacement in the y-direction and is assumed to be much smaller than the particle's size a, so that $\varepsilon = \xi/a \ll 1$.

The offset of the sphere's centroid and centre of mass is characterized by $\boldsymbol{\delta} = \mathbf{OG} = \delta\,\boldsymbol{d}$, where $\boldsymbol{d} = \cos\theta\,\boldsymbol{e}_x + \sin\theta\,\boldsymbol{e}_y$ (figure 1). The velocity of O and G in the laboratory reference frame are denoted by $\boldsymbol{V}_O$ and $\boldsymbol{V}_G$ and the angular velocity $\boldsymbol{\Omega}$ of the sphere is aligned with z-direction: $\boldsymbol{\Omega} = \dot{\theta}\,\boldsymbol{e}_z$ (i.e. we assume that the sphere's density distribution is symmetric with respect to the (Oxy)-plane). In the following, we make the additional assumption that the velocity of the particle is periodic for the zero-mean forcing flow $\boldsymbol{U}_e(t)$ considered (note, however, that its mean value is not necessarily zero so as to allow for self-propulsion regimes).

The objective of the present section is to derive the response of the sphere to the external flow in an unsteady Stokesian framework, where inertia of the fluid is negligible, but that of the solid particle is not.

2.2. *Momenta conservation*

The conservation of momentum in the (Galilean) frame of reference can be written

$$m_s\,\dot{\boldsymbol{V}}_G = \boldsymbol{F} + \boldsymbol{F}_p, \tag{2.2}$$

where the total force experienced by the sphere is the sum of the hydrodynamic force $\boldsymbol{F}$ due to the relative velocity between the sphere and the surrounding fluid, and of the pressure force $\boldsymbol{F}_p = \rho\mathcal{V}_s\,\dot{\boldsymbol{U}}_e$ arising from the external pressure gradient that sets the fluid in motion. Such a distinction is justified by the form of the viscous drag experienced by a solid sphere oscillating in an uniformly oscillating flow presented by Kim & Karrila (2005). Note that assuming that the velocity of the particle is periodic in time immediately implies that the time average of $\boldsymbol{F}(t)$ is zero.

Using $\boldsymbol{V}_G = \boldsymbol{V}_O - \boldsymbol{\delta} \times \boldsymbol{\Omega}$, and noting $\boldsymbol{V} = \boldsymbol{V}_O - \boldsymbol{U}_e$ the velocity of the sphere relative to the oscillating fluid, the previous equation can be rewritten as

$$\rho_s\mathcal{V}_s\dot{\boldsymbol{V}} = m_s\left[(\boldsymbol{\Omega}\times\boldsymbol{\delta})\times\boldsymbol{\Omega} + \boldsymbol{\delta}\times\dot{\boldsymbol{\Omega}}\right] + \boldsymbol{F} + (\rho - \rho_s)\mathcal{V}_s\dot{\boldsymbol{U}}_e, \tag{2.3}$$

where the last term is the effective buoyancy force.

Similarly, the conservation of angular momentum can be written about the centre of mass G,

$$I_G\,\dot{\boldsymbol{\Omega}} = \boldsymbol{L}_G, \tag{2.4}$$

where I_G is the moment of inertia of the sphere about the (G, z)-axis and $\boldsymbol{L}_G$ is the total torque experienced by the sphere at its centre of mass.

The sphere is rigid, thus $\boldsymbol{L}_G = \boldsymbol{L} + \mathbf{GO} \times (\boldsymbol{F} + \boldsymbol{F}_p)$, where $\boldsymbol{L}$ is the hydrodynamic torque about the geometric centre O, and (2.4) finally becomes

$$I_G\,\dot{\boldsymbol{\Omega}} = \boldsymbol{L} - \boldsymbol{\delta} \times (\boldsymbol{F} + \boldsymbol{F}_p). \tag{2.5}$$

2.3. *Dimensionless forms of the conservation laws*

In the following, using $U_e = \xi \varpi$ and ϖ^{-1} as reference velocity and time scales, respectively, yields the non-dimensional form of (2.3) and (2.5) (using lower-case letters for dimensionless variables)

$$\dot{\boldsymbol{v}} = \varepsilon^{-1} \alpha \; [(\boldsymbol{\omega} \times \boldsymbol{d}) \times \boldsymbol{\omega} + \boldsymbol{d} \times \dot{\boldsymbol{\omega}}] + \left(\frac{3}{4\pi} \frac{\beta}{\lambda^2} \right) \boldsymbol{f} + (\beta - 1) \boldsymbol{f}_e, \tag{2.6}$$

$$\dot{\boldsymbol{\omega}} = \left(\frac{15}{8\pi} \frac{\beta}{\lambda^2 I} \right) \boldsymbol{l} - \varepsilon \left[\left(\frac{15}{8\pi} \frac{\alpha\beta}{\lambda^2 I} \right) (\boldsymbol{d} \times \boldsymbol{f}) + \left(\frac{5}{2} \frac{\alpha\beta}{I} \right) (\boldsymbol{d} \times \boldsymbol{f}_e) \right], \tag{2.7}$$

with $\boldsymbol{f}_e = \mathrm{i}\,\mathrm{e}^{\mathrm{i}t}\,\boldsymbol{e}_y$ the fluctuating forcing.

In the above equations, the dimensionless moment of inertia $I = I_G/I_0$ is the ratio between the actual moment of inertia I_G and $I_0 = (2/5)\,m_s\,a^2$, the moment of inertia of a homogeneous sphere with the same mean density with respect to its centre. Further, $\alpha = \delta/a$ is the relative geometric offset of the particle's centre of mass and thus characterizes its non-homogeneity, $\beta = \rho/\rho_s$ is the fluid-to-solid average density ratio and $\lambda = (a^2 \varpi / \nu)^{1/2}$ is the ratio between the radius of the sphere and the viscous penetration length (i.e. λ^2 is the reduced frequency of actuation). It should be noted that the ε^{-1} factors are associated with the choice of characteristic velocity scale.

2.4. *Harmonic response in the unsteady Stokes limit*

The non-dimensional forcing field $\boldsymbol{f}_e = f_e \boldsymbol{e}_y$ with $f_e = \mathrm{i}\mathrm{e}^{\mathrm{i}t}$ is $O(\varepsilon^0)$ and harmonic; as a result, for $\varepsilon \ll 1$, the leading-order dynamics is obtained by noting that $v_y = O(1)$ while v_x and θ are $O(\varepsilon)$,

$$\dot{v}_x = \alpha \varepsilon^{-1} (\dot{\theta}^2 + \ddot{\theta}\theta) + \left(\frac{3}{4\pi} \frac{\beta}{\lambda^2} \right) f_x, \tag{2.8}$$

$$\dot{v}_y = -\alpha \varepsilon^{-1} \ddot{\theta} + \left(\frac{3}{4\pi} \frac{\beta}{\lambda^2} \right) f_y + (\beta - 1) f_e, \tag{2.9}$$

$$\ddot{\theta} = \left(\frac{15}{8\pi} \frac{\beta}{\lambda^2 I} \right) l - \varepsilon \left[\left(\frac{15}{8\pi} \frac{\alpha\beta}{\lambda^2 I} \right) f_y + \left(\frac{5}{2} \frac{\alpha\beta}{I} \right) f_e \right]. \tag{2.10}$$

In the unsteady Stokes limit, the total viscous force and torque on the sphere are obtained by superimposing that induced by the sphere's translation and rotation independently. By symmetry, the force induced by the sphere's rotation and the torque (about O) induced by the sphere's translation are both identically zero. Therefore, considering the form of the system (2.8)–(2.10) and according to Kim & Karrila (2005), one can write

$$v_x = \varepsilon \,\hat{v}_{0,x}\, \mathrm{e}^{2\mathrm{i}t}, \quad v_y = \hat{v}_{0,y}\, \mathrm{e}^{\mathrm{i}t}, \quad \theta = \varepsilon \,\hat{\theta}_0\, \mathrm{e}^{\mathrm{i}t} \tag{2.11a–c}$$

and

$$f_x = -\Delta_2 \, v_x, \quad f_y = -\Delta_1 \, v_y, \quad l = -\Lambda_1 \, \dot{\theta}, \tag{2.12a–c}$$

where the drag coefficients Δ_n and Λ_n are associated with harmonic translational or rotational motion of a sphere in unsteady viscous flows (see also § 3.4 Kim & Karrila (2005))

$$\Delta_n = 6\pi \left(1 + n^{1/2}\tilde{\lambda} + \frac{n\tilde{\lambda}^2}{9} \right) \quad \text{and} \quad \Lambda_n = 8\pi \frac{1 + n^{1/2}\tilde{\lambda} + \mathrm{i}\,n\tilde{\lambda}^2/3}{1 + n^{1/2}\tilde{\lambda}}, \tag{2.13a,b}$$

and $\tilde{\lambda} = \mathrm{e}^{\mathrm{i}\pi/4} \lambda$.

The leading-order dynamics $(\hat{v}_{0,y}, \hat{\theta}_0)$ is then obtained from the linear system

$$\left[\mathrm{i} + \left(\frac{3}{4\pi}\frac{\beta}{\lambda^2}\right)\Delta_1\right]\hat{v}_{0,y} - \alpha\,\hat{\theta}_0 = \mathrm{i}(\beta - 1), \tag{2.14}$$

$$\left(\frac{15}{8\pi}\frac{\alpha\beta}{\lambda^2 I}\right)\Delta_1\hat{v}_{0,y} + \left[1 - \mathrm{i}\left(\frac{15}{8\pi}\frac{\beta}{\lambda^2 I}\right)\Lambda_1\right]\hat{\theta}_0 = \mathrm{i}\left(\frac{5}{2}\frac{\alpha\beta}{I}\right). \tag{2.15}$$

It should be noted that the above dynamics is independent from that along the x-direction, which can be computed in a second step. The complex amplitude of the angular velocity $\hat{\omega}_0$ is then obtained using $\hat{\omega}_0 = \mathrm{i}\,\varepsilon\,\hat{\theta}_0$.

From the small and large λ approximations of Δ_1 and Λ_1, equations (2.14)–(2.15) can be used to obtain the following useful asymptotic forms of $\hat{v}_{0,y}$ and $\hat{\theta}_0$:

$$\hat{v}_{0,y} \sim \frac{2\mathrm{i}\lambda^2(\beta - 1)}{9\beta} \quad \text{and} \quad \hat{\theta}_0 \sim -\frac{\alpha\lambda^2}{6\beta} \quad \text{for } \lambda \to 0, \tag{2.16a,b}$$

$$\hat{v}_{0,y} \sim \frac{4I(\beta - 1) + 10\alpha^2\beta}{4I + \beta(2I + 5\alpha^2)} \quad \text{and} \quad \hat{\theta}_0 \sim \frac{15\mathrm{i}\alpha\beta}{4I + \beta(2I + 5\alpha^2)} \quad \text{for } \lambda \to \infty. \tag{2.17a,b}$$

3. Acoustic propulsion of the sphere

Knowing the leading-order viscous response of the sphere to the incident acoustic field, we now proceed to explore the possibility of achieving propulsion by means of streaming effects, by accounting for the first inertial correction to the flow field following the approach of Lippera *et al.* (2019).

3.1. *Governing equations*

By moving through the fluid, the sphere generates a flow field $\boldsymbol{u}(\boldsymbol{r}, t)$ around itself governed by the Navier–Stokes and continuity equations, which can be written in non-dimensional form in the frame of reference moving with the fluid far from the sphere as

$$\lambda^2\frac{\partial\boldsymbol{u}}{\partial t} + Re\,\boldsymbol{\nabla}\boldsymbol{u}\cdot\boldsymbol{u} = \boldsymbol{\nabla}\cdot\boldsymbol{\sigma}, \quad \boldsymbol{\nabla}\cdot\boldsymbol{u} = 0, \tag{3.1}$$

where $\boldsymbol{\sigma}$ is the non-dimensional hydrodynamic stress in the fluid due to the relative motion between the sphere and the surrounding fluid (and therefore includes a corrected pressure to account for the inertial corrections associated with the moving frame). It is recalled that, as in the previous section, all quantities are non-dimensional and a, ϖ^{-1} and $\xi\varpi$ are used as reference length, time and velocity scales, respectively. In (3.1), the Reynolds number is $Re = \varepsilon\lambda^2$ with $\varepsilon = \xi/a \ll 1$. In the following we thus focus on the limit of $Re \ll 1$, which yields the restriction $\lambda^2 \ll \varepsilon^{-1}$ for the following analysis. Note that Re is therefore not a new independent dimensionless group so that the problem is only governed by the five parameters ε, λ, α, β and I defined in the previous section, and listed in table 1.

The flow field vanishes at infinity and satisfies the no-slip boundary condition on the moving sphere ($|\boldsymbol{r}| = 1$ in a set of axes attached to the centroid of the sphere), therefore

$$\boldsymbol{u} = \boldsymbol{v} + \boldsymbol{\omega} \times \boldsymbol{r} \quad \text{for } |\boldsymbol{r}| = 1, \quad \boldsymbol{u} \to 0 \quad \text{for } |\boldsymbol{r}| \to \infty. \tag{3.2}$$

Parameters	Expression	Physical meaning
β	ρ/ρ_s	Fluid-to-solid density ratio
ε	ξ/a	Dimensionless displacement amplitude of the acoustic field
α	δ/a	Dimensionless imbalance parameter
I	I_G/I_0	Dimensionless moment of inertia
λ	$(\varpi a^2/\nu)^{1/2}$	Inverse of the dimensionless viscous length

TABLE 1. List of the five independent parameters of the problem. Note that the Reynolds number $Re = \varepsilon\lambda^2$, which is supposed to be small compared to unity, is not an independent parameter.

3.2. *Expansions in power of Re and order of the propulsion speed*

The Reynolds number, *Re*, is a small parameter of the problem, and we now expand the velocity field $\boldsymbol{u}$, the hydrodynamic stress $\boldsymbol{\sigma}$, and the velocity of the sphere $\boldsymbol{v}$ in powers of the Reynolds number

$$\boldsymbol{u} = \boldsymbol{u}^{(0)} + Re\,\boldsymbol{u}^{(1)} + \cdots, \quad \boldsymbol{\sigma} = \boldsymbol{\sigma}^{(0)} + Re\,\boldsymbol{\sigma}^{(1)} + \cdots, \quad \boldsymbol{v} = \boldsymbol{v}^{(0)} + Re\,\boldsymbol{v}^{(1)} + \cdots.$$
$$(3.3a-c)$$

We are interested in the emergence of a net propulsion of the sphere and therefore will focus on the existence of a steady component to the sphere's velocity. Due to the linearity of the unsteady Stokes equation, such steady motions have to be generated at order $O(Re)$ at least, which can be written $\overline{\boldsymbol{v}} = Re\,\langle\boldsymbol{v}^{(1)}\rangle$, where $\langle\cdots\rangle$ refers to the time average operator over a period of oscillation. In other words, the possibly non-zero $O(Re)$ steady component of the speed $\overline{\boldsymbol{v}}$ must be induced by the steady streaming flow resulting from the self-coupling of the $O(1)$ (i.e. $Re = 0$) viscous flow through the nonlinear term of the Navier–Stokes equation.

To obtain such a forcing, one could explicitly derive the steady streaming flow and integrate the corresponding hydrodynamic stress over the surface of the sphere. In order to circumvent such a cumbersome derivation, we use in the following a specific form of Lorentz reciprocal theorem suitable for the case where inertial corrections are considered (Ho & Leal 1974; Nadal & Lauga 2014; Lippera *et al.* 2019).

3.3. *Lorentz reciprocal theorem for inertial corrections*

To this end, we define the auxiliary flow and stress fields $(\boldsymbol{u}^\star, \boldsymbol{\sigma}^\star)$, as the unique solution of the following steady Stokes problem

$$\nabla \cdot \boldsymbol{\sigma}^\star = 0 \quad \text{and} \quad \nabla \cdot \boldsymbol{u}^\star = 0, \qquad (3.4a,b)$$

with boundary conditions

$$\boldsymbol{u}^\star = \boldsymbol{v}^\star + \boldsymbol{\omega}^\star \times \boldsymbol{r} \quad \text{at } |\boldsymbol{r}| = 1, \quad \boldsymbol{u}^\star \to 0 \quad \text{for } |\boldsymbol{r}| \to \infty. \qquad (3.5)$$

Using equations (3.1) and (3.4) and denoting by $\mathcal{V}$ the volume of fluid outside the sphere, one can write an instantaneous version of the Lorentz reciprocal theorem (for further details, see again Lippera *et al.* (2019)) in the following form:

$$\lambda^2 \int_{\mathcal{V}} \boldsymbol{u}^\star \cdot \frac{\partial \boldsymbol{u}}{\partial t}\, \mathrm{d}\mathcal{V} + Re \int_{\mathcal{V}} [\boldsymbol{u}^\star \cdot \nabla\boldsymbol{u} \cdot \boldsymbol{u}]\, \mathrm{d}\mathcal{V} = \boldsymbol{f}^\star \cdot \boldsymbol{v} + \boldsymbol{l}^\star \cdot \boldsymbol{\omega} - \boldsymbol{v}^\star \cdot \boldsymbol{f} - \boldsymbol{\omega}^\star \cdot \boldsymbol{l}, \qquad (3.6)$$

where f and l ($f^\star$ and $l^\star$, respectively) are the hydrodynamic force and torque in O for the real (respectively, auxiliary) problem. Because the particle is spherical, we immediately have $f^\star = -6\pi v^\star$ and $l^\star = -8\pi \omega^\star$ and (3.6) becomes

$$- (6\pi v + f) \cdot v^\star - (8\pi\omega + l) \cdot \omega^\star = \lambda^2 \frac{\mathrm{d}}{\mathrm{d}t} \left[\int_{\mathcal{V}} u^\star \cdot u \, \mathrm{d}\mathcal{V} \right] + Re \int_{\mathcal{V}} [u^\star \cdot \nabla u \cdot u] \, \mathrm{d}\mathcal{V}, \quad (3.7)$$

since $u^\star$ is time independent and $\mathcal{V}$ is fixed in time. It should be noted that up until now, no assumption on the magnitude of Re was used and the previous equation is therefore valid for any value of the Reynolds number.

Now, introducing (3.3) and the additional Re-expansions

$$f = f^{(0)} + Re f^{(1)} + \cdots, \quad l = l^{(0)} + Re l^{(1)} + \cdots \quad (3.8a,b)$$

for the force and torque into (3.7), and and identifying the $O(1)$ terms, leads to

$$- (6\pi v^{(0)} + f^{(0)}) \cdot v^\star - (8\pi\omega^{(0)} + l^{(0)}) \cdot \omega^\star = \lambda^2 \int_{\mathcal{V}} u^\star \cdot \frac{\partial u^{(0)}}{\partial t} \, \mathrm{d}\mathcal{V}. \quad (3.9)$$

Note that the right-hand side of (3.9) can be integrated provided assumptions on the harmonic nature of the $O(1)$ solution are formulated, in order to obtain the drag force and torque in unsteady Stokes flow ($Re = 0$, see § 3.4).

Considering now the $O(Re)$ terms in (3.7), the problem obtained at that order is structurally similar to that at $O(1)$ but for the emergence of an extra forcing that arises from and accounts for the effect of the streaming flow. Should a net self-propulsion occur (i.e. on average over a whole period of forcing), it would therefore be due to the streaming forcing, as anticipated. Taking the average in time of the resulting equation, one obtains

$$- v^\star \cdot \langle 6\pi v^{(1)} + f^{(1)} \rangle - \omega^\star \cdot \langle 8\pi\omega^{(1)} + l^{(1)} \rangle = \left\langle \int_{\mathcal{V}} [u^\star \cdot \nabla u^{(0)} \cdot u^{(0)}] \, \mathrm{d}\mathcal{V} \right\rangle = \mathcal{H}. \quad (3.10)$$

In order to derive the steady component of the propulsion speed $\overline{v} = Re \langle v^{(1)} \rangle$, our goal in the following lies in the computation of the right-hand side, $\mathcal{H}$, of the previous equality.

3.4. *Viscous drags and steady propulsion speed*

Knowing the form of the viscous dynamical response of the sphere $(\hat{v}_0, \hat{\omega}_0)$ from § 2, we are now able to derive an explicit expression of the propulsion speed $\overline{v}$. We first write $v^{(0)} = \hat{v}_0 \mathrm{e}^{\mathrm{i}t}$, $\omega^{(0)} = \hat{\omega}_0 \mathrm{e}^{\mathrm{i}t}$, $u^{(0)} = \hat{u}_0 \mathrm{e}^{\mathrm{i}t}$, $f^{(0)} = \hat{f}_0 \mathrm{e}^{\mathrm{i}t}$ and $l^{(0)} = \hat{l}_0 \mathrm{e}^{\mathrm{i}t}$.

In this context, the $O(1)$ and $O(Re)$ components of (3.9) and (3.10) become

$$-6\pi(\hat{v}_0 + \hat{f}_0) \cdot v^\star - (8\pi\hat{\omega}_0 + \hat{l}_0) \cdot \omega^\star = \lambda^2 \int_{\mathcal{V}} u^\star \cdot \frac{\partial \hat{u}_0}{\partial t} \, \mathrm{d}\mathcal{V}, \quad (3.11)$$

$$-v^\star \cdot \langle 6\pi v^{(1)} + f^{(1)} \rangle - \omega^\star \cdot \langle 8\pi\omega^{(1)} + l^{(1)} \rangle = \frac{1}{2} \mathrm{Re} \left\{ \int_{\mathcal{V}} [u^\star \cdot \nabla \hat{u}_0^\dagger \cdot \hat{u}_0] \, \mathrm{d}\mathcal{V} \right\} = \mathcal{H}, \quad (3.12)$$

where $\mathrm{Re}(z)$ and $z^\dagger$ stand for the real part and complex conjugate of z.

In the case of an harmonic motion, $\hat{u}_0$ is given by

$$\hat{u}_0 = [A(r)I + B(r)nn] \cdot \hat{v}_0 + C(r) \hat{\omega}_0 \times n, \quad (3.13)$$

where the exact forms for given λ of $A(r)$, $B(r)$ and $C(r)$ are recalled in appendix A (see also chapter 6 in Kim & Karrila (2005)). The velocity field induced by a rectilinear steady motion of a sphere in a viscous fluid has a form similar to (3.13),

$$\boldsymbol{u}^{\star} = \left[A^{\star}(r)\boldsymbol{I} + B^{\star}(r)\boldsymbol{nn}\right] \cdot \boldsymbol{v}^{\star} + C^{\star}(r)\,\boldsymbol{\omega}^{\star} \times \boldsymbol{n}, \tag{3.14}$$

where the exact forms of $A^{\star}(r)$, $B^{\star}(r)$ and $C^{\star}(r)$ are also given in appendix A, and are in fact the asymptotic limits of A, B and C for $\lambda \to 0$ (steady motion), respectively.

3.4.1. *Order $O(1)$ – Viscous response*

Successively introducing the auxiliary fields $(\boldsymbol{v}^{\star}, \boldsymbol{\omega}^{\star}) = (\boldsymbol{e}_y, 0)$ and $(\boldsymbol{v}^{\star}, \boldsymbol{\omega}^{\star}) = (0, \boldsymbol{e}_z)$ in (3.11) provides

$$\hat{\boldsymbol{f}}_0 = -[6\pi + \tilde{\lambda}^2 F(\lambda)]\,\hat{\boldsymbol{v}}_0, \quad \hat{\boldsymbol{l}}_0 = -[8\pi + \tilde{\lambda}^2 G(\lambda)]\,\hat{\boldsymbol{\omega}}_0, \tag{3.15a,b}$$

with

$$F(\lambda) = 4\pi \int_1^{\infty} r^2 \left[\frac{2AA^{\star} + (A+B)(A^{\star}+B^{\star})}{3}\right]\,\mathrm{d}r, \quad G(\lambda) = \frac{8\pi}{3}\int_1^{\infty} r^2 CC^{\star}\,\mathrm{d}r \tag{3.16a,b}$$

and $\tilde{\lambda}^2 = i\lambda^2$. One can note that computing the integrals on the right-hand sides of (3.16) indeed provides the classical expressions derived for the unsteady translational and rotational drag (Stokes 1850; Mazur & Bedeaux 1974; Kim & Karrila 2005)

$$\hat{\boldsymbol{f}}_0 = -6\pi \left(1 + \tilde{\lambda} + \frac{\tilde{\lambda}^2}{9}\right)\hat{\boldsymbol{v}}_0, \quad \hat{\boldsymbol{l}}_0 = -8\pi \frac{1 + \tilde{\lambda} + \tilde{\lambda}^2/3}{1 + \tilde{\lambda}}\,\hat{\boldsymbol{\omega}}_0. \tag{3.17a,b}$$

3.4.2. *Order $O(Re)$ – Propulsion speed*

Let us turn to the leading-order mean propulsion speed $\overline{\boldsymbol{v}}$. Using (3.13),

$$\nabla\hat{\boldsymbol{u}}_0 = A'\hat{\boldsymbol{v}}_0\boldsymbol{n} + B'(\boldsymbol{n}\cdot\hat{\boldsymbol{v}}_0)\boldsymbol{nn} + \frac{B}{r}\left\{(\boldsymbol{n}\cdot\hat{\boldsymbol{v}}_0)(\boldsymbol{I}-\boldsymbol{nn}) + \boldsymbol{n}\otimes[(\boldsymbol{I}-\boldsymbol{nn})\cdot\hat{\boldsymbol{v}}_0]\right\}$$
$$+ C'(\hat{\boldsymbol{\omega}}_0\times\boldsymbol{n})\otimes\boldsymbol{n} - \frac{C}{r}\left[\boldsymbol{\epsilon}\cdot\hat{\boldsymbol{\omega}}_0 + (\hat{\boldsymbol{\omega}}_0\times\boldsymbol{n})\otimes\boldsymbol{n}\right], \tag{3.18}$$

where $C' = \mathrm{d}C/\mathrm{d}r$ and $(\boldsymbol{\epsilon})_{ijk} = \epsilon_{ijk}$, so that $(\boldsymbol{\epsilon}\cdot\boldsymbol{\omega}_0)\cdot\boldsymbol{a} = \boldsymbol{a}\times\boldsymbol{\omega}_0$ for any vector $\boldsymbol{a}$. Introducing equations (3.13), (3.14) and (3.18) in (3.12) and performing the explicit integration of its right-hand side leads to

$$\mathcal{H} = \frac{2\pi}{3}\mathrm{Re}\left\{\left[\boldsymbol{v}^{\star}\cdot(\hat{\boldsymbol{\omega}}_0\times\hat{\boldsymbol{v}}_0^{\dagger})\right]\mathcal{I}(\tilde{\lambda})\right\}, \tag{3.19}$$

where the quantity

$$\mathcal{I}(\tilde{\lambda}) = \int_1^{\infty}\left[A^{\star}\left(A^{\dagger}C' + B^{\dagger}C' + \frac{2A^{\dagger}C}{r}\right) + \frac{B^{\star}(A^{\dagger}-B^{\dagger})C}{r}\right]r^2\,\mathrm{d}r \tag{3.20}$$

is given in its fully integrated form in appendix B and its variations are indicated on figure 2. In particular, for small and large λ, the asymptotic behaviour of $\mathcal{I}$ is obtained as

$$\mathcal{I}(\lambda \to 0) = -\frac{1}{4}, \quad \mathcal{I}(\lambda \to \infty) = -1. \tag{3.21a,b}$$
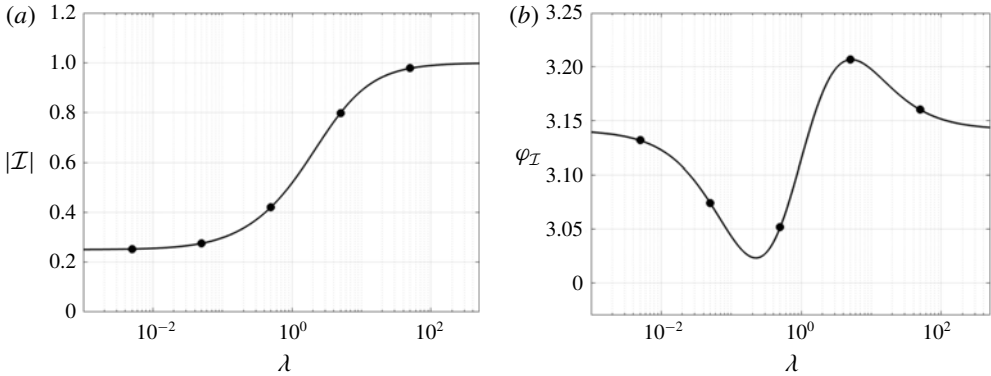
FIGURE 2. Magnitude (*a*) and phase (*b*) of $\mathcal{I}$. The bullets correspond to the direct numerical integration of (3.20).

Note that (3.19) confirms that the *x*-component of $\hat{\boldsymbol{v}}_0$ will have no contribution to the steady motion, as anticipated in §2 and expected for symmetry reasons.

Now, choosing $\boldsymbol{v}^{\star} = \boldsymbol{e}_x$ and $\boldsymbol{\omega}^{\star} = 0$ in (3.12) and (3.19), and remembering that (i) using (2.11), only the *y*-component of $\hat{\boldsymbol{v}}_0$ has a non-zero contribution to the mean propulsion speed, (ii) $\hat{\boldsymbol{\omega}}_0$ is along the *z*-axis, and (iii) $\langle \boldsymbol{f} \rangle = 0$ due to the periodicity of the particle's velocity, one obtains

$$\langle \boldsymbol{v}^{(1)} \rangle = \langle v^{(1)} \rangle \, \boldsymbol{e}_x = \tfrac{1}{9} \mathrm{Re}[\hat{\omega}_0 \, \hat{v}_{0,y}^{\dagger} \, \mathcal{I}(\tilde{\lambda})] \, \boldsymbol{e}_x, \qquad (3.22)$$

or equivalently, as a function of the tilt angle amplitude,

$$\langle \boldsymbol{v}^{(1)} \rangle = -\tfrac{1}{9} \, \varepsilon \, \mathrm{Im}[\hat{\theta}_0 \, \hat{v}_{0,y}^{\dagger} \, \mathcal{I}(\tilde{\lambda})] \, \boldsymbol{e}_x, \qquad (3.23)$$

where $\mathrm{Im}(z)$ refers to the imaginary part of z.

Note that the ratio $\langle v^{(1)} \rangle / \varepsilon$, which is a function of the four dimensionless parameters α, β, I and λ, does not depend on ε. As a result, the leading-order dimensionless mean velocity of the particle $\overline{\boldsymbol{v}}$ is the product of $\varepsilon \, Re$ and of a dimensionless function of the four other parameters. The quantity $\langle v^{(1)} \rangle / \varepsilon$ is plotted in 3 for $\beta = 0.2$ and different combinations (I, α).

3.5. *Asymptotic behaviour and reversal of the propulsion speed*

As shown in figure 3, for large α or small I, a reversal of the direction of propulsion (illustrated by the diagrams inserted in each subfigure) can be observed at a finite value $\lambda^{\star}$ of the reduced frequency λ. This reversal in swimming direction is not the result of the difference in behaviour of the streaming flows at low and high frequencies, and is instead entirely due to a change by a factor of π in the relative phase between translation and rotation in the viscous (i.e. $Re = 0$) response of the forced sphere.

The variations of $\lambda^{\star}(\beta, I, \alpha)$ are plotted in figure 4, for three different values of the density ratio β. In each case, the (I, α)-plane is divided into two regions: a first one where a reversal of the direction of propulsion can be observed at finite λ, and another one, where the direction of propulsion does not depend on λ (in the latter

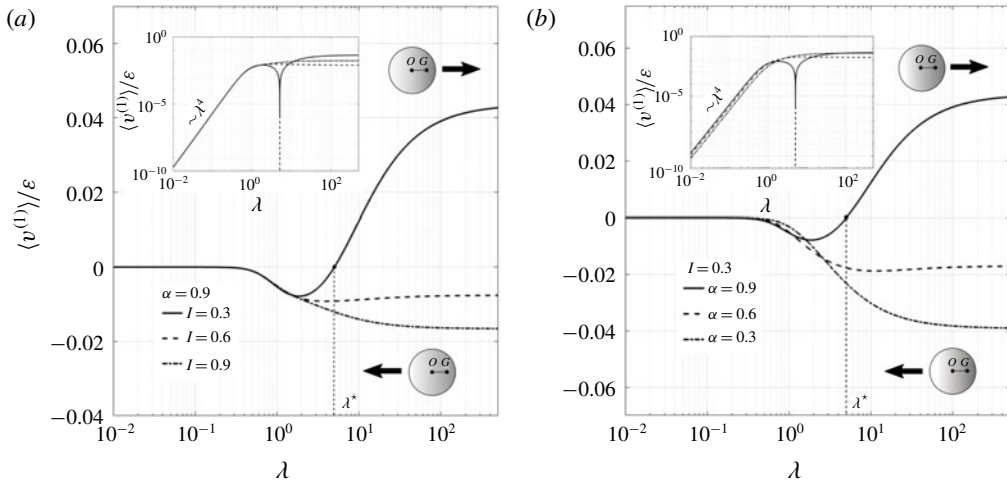FIGURE 3. Ratio $\langle v^{(1)} \rangle / \varepsilon$ as a function of λ for $\beta = 0.2$ and several combinations of (I, α). (a) $\alpha = 0.9$, $I = 0.3, 0.6, 0.9$; (b) $I = 0.3$, $\alpha = 0.3, 0.6, 0.9$. The spheres sketched in panels (a) and (b) illustrate the direction of propulsion when the centre of mass is on the right of the geometric centre (top, $\langle v^{(1)} \rangle / \varepsilon > 0$; bottom, $\langle v^{(1)} \rangle / \varepsilon < 0$).

case, the sphere always propels with the light end ahead). The limit between the two regions (i.e. a criterion for existence of the reversal in swimming direction between small and large λ) can be obtained by deriving the asymptotic behaviour of $\langle v^{(1)} \rangle$ at small and large λ. Substituting the result of (2.16), (2.17) and (3.21) into (3.23), one obtains

$$\langle v^{(1)} \rangle \sim \frac{\varepsilon \alpha \lambda^4 (\beta - 1)}{972 \beta^2} \quad \text{for } \lambda \to 0, \tag{3.24}$$

$$\langle v^{(1)} \rangle \sim \frac{10 \varepsilon \alpha \beta [2I(\beta - 1) + 5\alpha^2 \beta]}{3[4I + \beta(2I + 5\alpha^2)]^2} \quad \text{for } \lambda \to \infty. \tag{3.25}$$

A change in swimming direction between the $\lambda \ll 1$ and $\lambda \gg 1$ limits therefore requires $\beta - 1$ and $2I(\beta - 1) + 5\alpha^2 \beta$ to have opposite signs, or equivalently

$$0 \leqslant \frac{2(1 - \beta)}{5\beta} \leqslant \frac{\alpha^2}{I}. \tag{3.26}$$

This is consistent with the results shown in figure 4 where the red line corresponds to the equality case above. The presence of a white zone in figure 4(a–c), where $\lambda^\star$ is not computed, comes from the practical limitation in the numerical extraction of $\lambda^\star$ which tends to infinity in the vicinity of the transition region (red line). This region would be reduced if the upper bound of the research interval in λ was enlarged. This has been verified for the value $\beta = 0.05$, for which the white zone barely exists. Note that the reversal is only possible if $\beta \leqslant 1$ (i.e. the particle must be heavier, on average, than the fluid) and if a sufficiently large inhomogeneity exists (as measured by α).
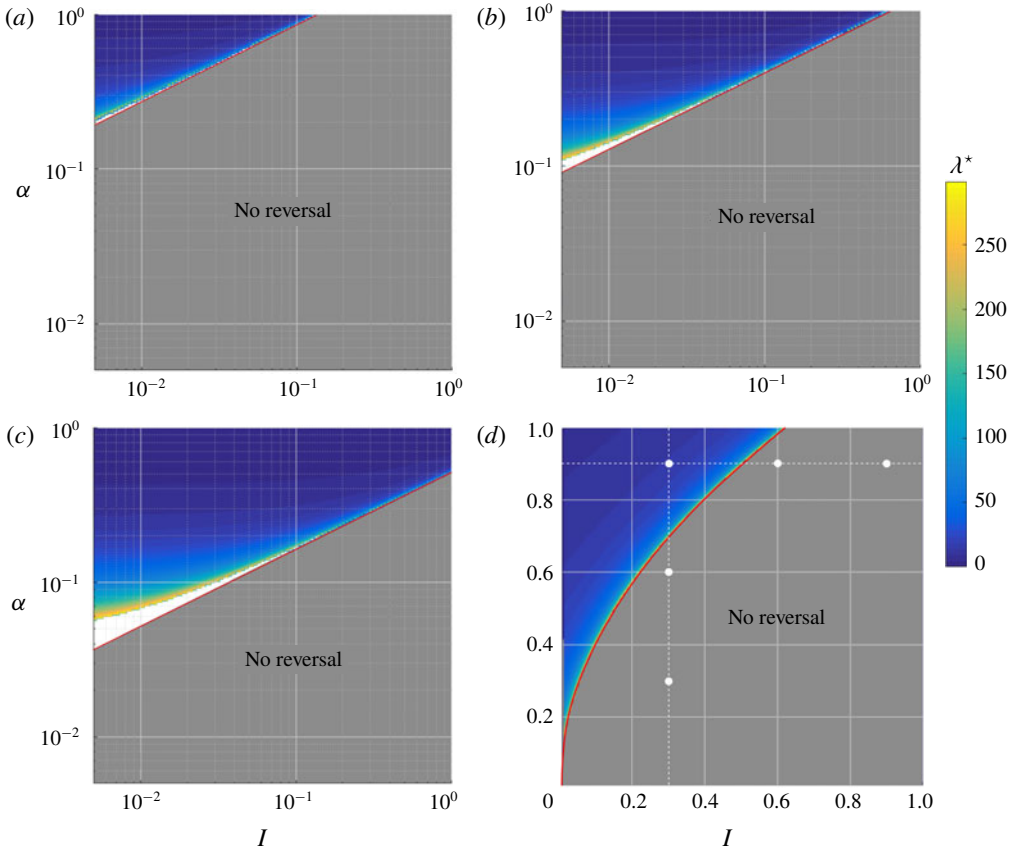
FIGURE 4. Value $\lambda^\star$ corresponding to a reversal of the propulsion direction plotted in the plane (I, α) for three values of β. (a) $\beta = 0.05$; (b,d) $\beta = 0.2$ (panel d is the same as panel b but plotted in a linear scale); (c) $\beta = 0.6$. For a fixed value of β, the frontier between the reversal and the non-reversal regions is given by the equality case of (3.26) (solid red line). The cases considered in figure 3 are specified on panel (d) using white bullets. The colour bar (right) holds for all the figures. The white zones in panels (a), (b) and (c), where $\lambda^\star$ is not computed, come from the practical limitation in the numerical extraction of $\lambda^\star$ which tends to infinity in the vicinity of the transition (see text for further explanation).

4. Physical discussion and orders of magnitude

The dimensional form of (3.23) is

$$\overline{V} = \xi \varpi \, \overline{v} = -\frac{\xi^3 \varpi^2}{9\nu} \, \text{Im}[\hat{\theta}_0 \, \hat{v}_0^\dagger \, \mathcal{I}(\tilde{\lambda})], \tag{4.1}$$

where it should be noted that the radius of the particle only appears through λ (and not in the prefactor).

Based on a mean value of the quality factor of the acoustic cavity $Q \sim 300$ (see Bruss (2012)) and a typical displacement of the piezoelectric wall $\ell \sim 0.1$ nm, a maximum value for the displacement amplitude at the pressure node can be estimated as $\xi = 2Q\ell/\pi \sim 19$ nm. For a typical particle radius $a = 0.5$ µm and forcing
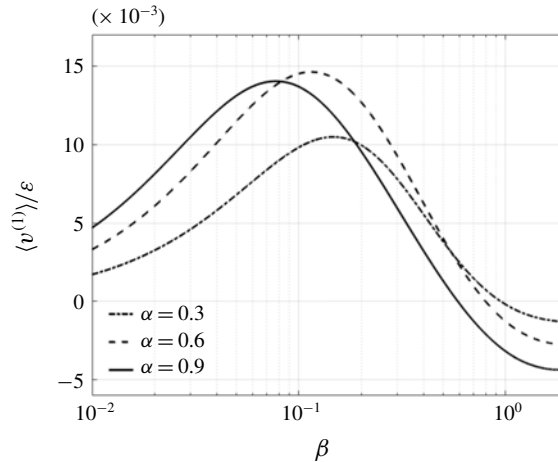
FIGURE 5. (*a*) Ratio $\langle v^{(1)} \rangle / \varepsilon$ as a function of β for $\lambda = 2.5$, $I = 0.9$ and different values of α.

frequency of 4 MHz, corresponding, respectively, to $\varepsilon = 0.038$ and $\lambda \simeq 2.5$, a value of $|\langle v^{(1)} \rangle| / \varepsilon \sim 0.01$ is a reasonable estimate of the particle's dimensionless velocity (see figure 3) and one obtains dimensionally

$$\overline{V} \sim 44 \ \mu\text{m s}^{-1}, \tag{4.2}$$

which is consistent with the values reported by Ahmed *et al.* (2016). A quality factor of 10^3 (upper bound measured in standard acoustic resonators, see again Bruss (2012)) would have led to a propulsion velocity $\overline{V} \simeq 1.6 \ \text{mm s}^{-1}$, which is much larger than the values reported by Ahmed *et al.* (2016) or Wang *et al.* (2012) (the latter reports a maximum value of 200 $\mu\text{m s}^{-1}$), but is not inconsistent with the velocities measured by Kaynak *et al.* (2017). A quality factor of 10^2 (lower bound measured in standard acoustic resonators) would yield $\overline{V} \simeq 1.6 \ \mu\text{m s}^{-1}$.

In brief, even if the orders of magnitude of propulsion speed produced by the model are not irrelevant to the measurements, performing a quantitative comparison remains difficult because (i) the spherical geometry of our model noticeably departs from the experimental geometry depicted in Wang *et al.* (2012) and Ahmed *et al.* (2016) and (ii) the quality factor of the experimental acoustic cavities used by Wang *et al.* (2012) and Ahmed *et al.* (2016) is not known, whereas it critically impacts the estimate of the velocity.

The profile of the quantity $\langle v^{(1)} \rangle / \varepsilon$ with respect to the density ratio β, for $\lambda = 2.5$, $I = 0.9$ and different values of the parameter α is plotted in figure 5. As mentioned by Ahmed *et al.* (2016), homogeneous rhodium rods ($\beta = 0.081$) were faster than heavier golden ones ($\beta = 0.052$), an observation which is again consistent with the values presented in the figure.

A final practical yet fundamental remark must be made regarding the zero mean value of the tilt angle. Indeed, we assumed here that the tilt angle varied periodically around the value $\theta = 0$ in the permanent regime (no angular drift). This assumption is not *a priori* fully justified since the radiation pressure on a sphere has no obvious orientation effect. In contrast, a near-sphere or an ellipsoid will orient itself in such a way that, on average, its major axis would lie in the zero-pressure plane of the

wave. Therefore, the present calculation can be seen as the leading-order calculation of the acoustic propulsion of a non-homogeneous near-sphere, since a slight alteration of the shape would not modify the propulsion speed obtained at leading order for a non-homogeneous sphere.

5. Conclusion

We present here a full derivation of the acoustic propulsion speed of a non-homogeneous rigid sphere. Unlike previous studies which generally rely on a numerically integrated result, the final result obtained by means of the inertial version of the Lorentz reciprocal theorem is integrated analytically. The problem is ruled by five independent dimensionless parameters: the inhomogeneity ratio or imbalance distance α; the fluid/solid density ratio β; the dimensionless moment of inertia I; the dimensionless forcing amplitude ε; and the reduced frequency λ^2. For a given density ratio $\beta \leqslant 1$, a limit value $\lambda^\star$ of the parameter λ may exist such that propulsion takes place in different directions at low frequency ($\lambda < \lambda^\star$) and high frequency ($\lambda > \lambda^\star$). A necessary and sufficient condition for the existence of a reversal in the propulsion direction for varying λ was obtained as $0 \leqslant (2/5)[(1-\beta)/\beta] \leqslant \alpha^2/I$.

The trends of the propulsion speed as a function of λ as well as the possible existence of a change in propulsion direction for $\lambda = \lambda^\star$ are fully consistent with the results published by Collis *et al.* (2017). As expected, in a case where the reversal value $\lambda^\star$ does exist (see figure 3), propulsion occurs at low frequency (small λ) in the direction of the lighter part of the sphere (centre of mass behind the centroid) whereas at higher frequency (large λ), the inhomogeneous sphere propels with the centre of mass ahead. The dependence of the propulsion speed amplitude upon the density ratio is non-monotonous and at high mean densities (typically for $\beta < 0.1$), light particles propel faster than heavier ones. Yet, one should be cautious in connecting this result to the observation reported by Ahmed *et al.* (2016) on density effects. Indeed, Ahmed *et al.* (2016) report that lighter rods propel faster than denser ones, but the rods also display a geometric asymmetry which could play a central role as well. In order to test more thoroughly the model, dedicated experiments performed using low aspect ratio solid particles with controlled density inhomogeneities would be enlightening.

Declaration of interests

The authors report no conflict of interest.

Appendix A. Definition of the coefficients A, $A^\star$, B, $B^\star$, C and $C^\star$

The full expressions of the coefficients A, B and C of the unsteady harmonic Stokes flow in (3.13) are given by

$$A(r) = \frac{3}{2\tilde{\lambda}^2 r^3}\left[(1 + \tilde{\lambda}r + \tilde{\lambda}^2 r^2)e^{\tilde{\lambda}(1-r)} - 1 - \tilde{\lambda} - \frac{\tilde{\lambda}^2}{3}\right], \qquad (A1)$$

$$B(r) = \frac{3}{2\tilde{\lambda}^2 r^3}\left[3 + 3\tilde{\lambda} + \tilde{\lambda}^2 - (3 + 3\tilde{\lambda}r + \tilde{\lambda}^2 r^2)e^{\tilde{\lambda}(1-r)}\right], \tag{A 2}$$

$$C(r) = \frac{e^{\tilde{\lambda}(1-r)}(1 + \tilde{\lambda}r)}{(1 + \tilde{\lambda})r^2}, \tag{A 3}$$

where $\tilde{\lambda} = \lambda e^{i\pi/4}$, and the corresponding coefficients $A^\star$, $B^\star$ and $C^\star$ of the auxiliary steady Stokes flow in (3.14) are given by

$$A^\star(r) = \frac{3}{4r} + \frac{1}{4r^3}, \quad B^\star(r) = \frac{3}{4r} - \frac{3}{4r^3}, \quad C^\star(r) = \frac{1}{r^2}. \tag{A 4a–c}$$

Appendix B. Integration of the streaming term $\mathcal{H}$ in the harmonic case

We note here $J(r)$ the integrand in the right-hand side of (3.20), namely

$$J(r) = \left[A^\star\left(A^\dagger C' + B^\dagger C' + \frac{2A^\dagger C}{r}\right) + \frac{B^\star(A^\dagger - B^\dagger)C}{r}\right]r^2 \tag{B 1}$$

which can be rewritten explicitly as

$$
\begin{aligned}
J(r) = {} & \frac{1}{4\tilde{\lambda}^{\dagger 2}(1 + \tilde{\lambda})}\left[e^{\tilde{\lambda}(1-r)}(\tilde{\lambda}^{\dagger 2} + 3\tilde{\lambda}^\dagger + 3)\left(-\frac{3\tilde{\lambda}^2}{r^3} - \frac{15\tilde{\lambda}}{r^4} + \frac{3\tilde{\lambda}}{r^6} + \frac{3}{r^7} - \frac{\tilde{\lambda}^2 + 15}{r^5}\right)\right. \\
& + 3e^{(\tilde{\lambda}+\tilde{\lambda}^\dagger)(1-r)}\left(\frac{3\tilde{\lambda}\tilde{\lambda}^\dagger(\tilde{\lambda} + 2\tilde{\lambda}^\dagger)}{r^2} + \frac{3(\tilde{\lambda}^2 + 5\tilde{\lambda}\tilde{\lambda}^\dagger + 2\tilde{\lambda}^{\dagger 2})}{r^3}\right. \\
& + \frac{\tilde{\lambda}^2\tilde{\lambda}^\dagger - 2\tilde{\lambda}\tilde{\lambda}^{\dagger 2} + 15\tilde{\lambda} + 15\tilde{\lambda}^\dagger}{r^4} \\
& \left.\left. + \frac{\tilde{\lambda}^2 - 3\tilde{\lambda}\tilde{\lambda}^\dagger - 2\tilde{\lambda}^{\dagger 2} + 15}{r^5} - \frac{3(\tilde{\lambda} + \tilde{\lambda}^\dagger)}{r^6} - \frac{3}{r^7}\right)\right].
\end{aligned}
\tag{B 2}
$$

So that $\mathcal{I}(\tilde{\lambda}) = \int_1^\infty J(r)\,dr$ is obtained analytically as

$$
\begin{aligned}
\mathcal{I}(\tilde{\lambda}) = {} & \frac{1}{4\tilde{\lambda}^{\dagger 2}(1 + \tilde{\lambda})}\left\{(\tilde{\lambda}^{\dagger 2} + 3\tilde{\lambda}^\dagger + 3)\left[-3\tilde{\lambda}^2 I_3 - 15\tilde{\lambda}I_4 + 3\tilde{\lambda}I_6 + 3I_7 - (\tilde{\lambda}^2 + 15)I_5\right]\right. \\
& + 3\left[3\tilde{\lambda}\tilde{\lambda}^\dagger(\tilde{\lambda} + 2\tilde{\lambda}^\dagger)\tilde{I}_2 + 3(\tilde{\lambda}^2 + 5\tilde{\lambda}\tilde{\lambda}^\dagger + 2\tilde{\lambda}^{\dagger 2})\tilde{I}_3\right. \\
& + (\tilde{\lambda}^2\tilde{\lambda}^\dagger - 2\tilde{\lambda}\tilde{\lambda}^{\dagger 2} + 15\tilde{\lambda} + 15\tilde{\lambda}^\dagger)\tilde{I}_4 \\
& \left.\left. + (\tilde{\lambda}^2 - 3\tilde{\lambda}\tilde{\lambda}^\dagger - 2\tilde{\lambda}^{\dagger 2} + 15)\tilde{I}_5 - 3(\tilde{\lambda} + \tilde{\lambda}^\dagger)\tilde{I}_6 - 3\tilde{I}_7\right]\right\}
\end{aligned}
\tag{B 3}
$$

with

$$I_1 = \int_1^\infty \frac{e^{\tilde{\lambda}(1-r)}}{r}\,dr = e^{\tilde{\lambda}}E_1(\tilde{\lambda}), \tag{B 4}$$

$$\tilde{I}_1 = \int_1^\infty \frac{e^{(\tilde{\lambda}+\tilde{\lambda}^\dagger)(1-r)}}{r}\,dr = e^{(\tilde{\lambda}+\tilde{\lambda}^\dagger)}E_1(\tilde{\lambda} + \tilde{\lambda}^\dagger), \tag{B 5}$$

$$I_n = \int_1^\infty \frac{e^{\tilde{\lambda}(1-r)}}{r^n}\, dr = \frac{1}{n-1}(1 - \tilde{\lambda}I_{n-1}), \tag{B 6}$$

$$\tilde{I}_n = \int_1^\infty \frac{e^{(\tilde{\lambda}+\tilde{\lambda}^\dagger)(1-r)}}{r^n}\, dr = \frac{1}{n-1}[1 - (\tilde{\lambda}+\tilde{\lambda}^\dagger)\tilde{I}_{n-1}], \tag{B 7}$$

which are well defined since $\tilde{\lambda}$ has positive real part. In the above equation, $E_1(z)$ is the exponential integral (Abramowitz & Stegun 1964). Using these results, one obtains $\mathcal{I}$ analytically for any λ

$$
\begin{aligned}
\mathcal{I}(\tilde{\lambda}) ={}& \frac{1}{64\tilde{\lambda}^\dagger(1+\tilde{\lambda})}\big[(\tilde{\lambda}^\dagger + 3)\tilde{\lambda}^5 - \tilde{\lambda}^\dagger\tilde{\lambda}^4 + (2\tilde{\lambda}^\dagger - 18)\tilde{\lambda}^3 \\
&- 6\tilde{\lambda}^{\dagger 2}\tilde{\lambda}^2 + (-3\tilde{\lambda}^{\dagger 3} + 6\tilde{\lambda}^{\dagger 2} - 16\tilde{\lambda}^\dagger)\tilde{\lambda} + 3\tilde{\lambda}^{\dagger 4} - 3\tilde{\lambda}^{\dagger 3} - 48\tilde{\lambda}^{\dagger 2} - 16\tilde{\lambda}^\dagger\big] \\
&- \frac{e^{\tilde{\lambda}}E_1(\tilde{\lambda})}{64\tilde{\lambda}^{\dagger 2}(1+\tilde{\lambda})}\big[(\tilde{\lambda}^{\dagger 2} + 3\tilde{\lambda}^\dagger + 3)(\tilde{\lambda}^6 - 6\tilde{\lambda}^4)\big] \\
&+ \frac{3e^{\tilde{\lambda}+\tilde{\lambda}^\dagger}E_1(\tilde{\lambda}+\tilde{\lambda}^\dagger)}{64\tilde{\lambda}^{\dagger 2}(1+\tilde{\lambda})}(\tilde{\lambda}+\tilde{\lambda}^\dagger)(\tilde{\lambda}-\tilde{\lambda}^\dagger)[\tilde{\lambda}^4 - 2\tilde{\lambda}^2\tilde{\lambda}^{\dagger 2} - 6\tilde{\lambda}^2 + \tilde{\lambda}^{\dagger 4} - 18\tilde{\lambda}^{\dagger 2}]. \tag{B 8}
\end{aligned}
$$

Real and imaginary parts and phase of $\mathcal{I}$ are presented in figure 2. The asymptotic forms of $\mathcal{I}$ at small and large λ, equation (3.21), are obtained using the following asymptotic limits (Abramowitz & Stegun 1964)

$$E_1(z \to 0) \sim -\ln z - \gamma, \quad E_1(z \to \infty) \sim \frac{e^{-z}}{z}. \tag{B 8a,b}$$

REFERENCES

ABRAMOWITZ, M. & STEGUN, I. A. 1964 *Handbook of Mathematical Functions with Formulas, Graphs, and Mathematical Tables.* Dover.

AHMED, S., GENTEKOS, D. T., FINK, C. A. & MALLOUK, T. E. 2014 Self-assembly of nanorod motors into geometrically regular multimers and their propulsion by ultrasound. *ACS Nano* **8** (11), 11053–11060.

AHMED, S., WANG, W., BAI, L., GENTEKOS, D. T., HOYOS, M. & MALLOUK, T. E. 2016 Density and shape effects in the acoustic propulsion of bimetallic nanorod motors. *ACS Nano* **10** (4), 4763–4769.

ANDERSON, J. L. 1989 Colloid transport by interfacial forces. *Annu. Rev. Fluid Mech.* **21**, 61–99.

BARABAN, L., STREUBEL, R., MAKAROV, D., HAN, L., KARNAUSHENKO, D., SCHMIDT, O. G. & CUNIBERTI, G. 2012 Fuel-free locomotion of janus motors: magnetically induced thermophoresis. *ACS Nano* **7**, 1360–1367.

BRUSS, H. 2012 Acoustofluidics 2: perturbation theory and ultrasound resonance modes. *Lab on a Chip* **12**, 20–28.

BURDICK, J., LAOCHAROENSHUK, R., WHEAT, P. M., POSNER, J. D. & WANG, J. 2008 Synthetic nanomotors in microchannel networks: directional microchip motion and controlled manipulation of cargo. *J. Am. Chem. Soc.* **130**, 8164–8165.

CAMPUZANO, S., KAGAN, D., OROZCO, J. & WANG, J. 2011 Motion-driven sensing and biosensing using electrochemically propelled nanomotors. *Analyst* **136**, 4621–4630.

COLLIS, J., JESSE, F., CHAKRABORTY, D. & SADER, J. E. 2017 Autonomous propulsion of nanorods trapped in an acoustic field. *J. Fluid Mech.* **825**, 29–48.

CORDOVA-FIGUEROA, U. M. & BRADY, J. F. 2008 Osmotic propulsion: the osmotic motor. *Phys. Rev. Lett.* **100** (15), 158303.

EBBENS, S. J. & HOWSE, J. R. 2010 In pursuit of propulsion at the nanoscale. *Soft Matt.* **6**, 726–738.

EBBENS, S. J. & HOWSE, J. R. 2011 Direct observation of the direction of motion for spherical catalytic swimmers. *Langmuir* **27**, 12293–12296.

GOLESTANIAN, R., LIVERPOOL, T. B. & AJDARI, A. 2007 Designing phoretic micro- and nano-swimmers. *New J. Phys.* **9**, 126.

HO, B. P. & LEAL, L. G. 1974 Inertial migration of rigid spheres in two-dimensional unidirectional flows. *J. Fluid Mech.* **65** (2), 365–400.

IBELE, M. E., WANG, Y., KLINE, T. R., MALLOUK, T. E. & SEN, A. 2007 Hydrazine fuels for bimetallic catalytic microfluic pumping. *J. Am. Chem. Soc.* **129** (25), 7762–7763.

JIANG, H. R., YOSHINAGA, N. & SANO, M. 2010 Active motion of a janus particle by self-thermophoresis in a defocused laser beam. *Phys. Rev. Lett.* **105**, 268302.

KAYNAK, M., OZCELIK, A., NOURHANI, A., LAMMERT, P. E., CRESPI, V. H. & HUANG, T. J. 2017 Acoustic actuation of bioinspired microswimmers. *Lab on a Chip* **17**, 395–400.

KIM, S. & KARRILA, S. J. 2005 *Microhydrodynamics*. Dover Publication, Inc.

LAUGA, E. & POWERS, T. 2009 The hydrodynamics of swimming microorganisms. *Rep. Prog. Phys.* **72**, 096601.

LIPPERA, K., DAUCHOT, O., MICHELIN, S. & BENZAQUEN, M. 2019 No net motion for oscillating near-spheres at low *Re* numbers. *J. Fluid Mech.* **866**, R1.

MAZUR, P. & BEDEAUX, D. 1974 A generalization of Faxén's theorem to nonsteady motion of a sphere through an incompressible fluid in arbitrary flow. *Physica* D **76**, 235–246.

NADAL, F. & LAUGA, E. 2014 Asymmetric steady streaming as a mechanism for acoustic propulsion of rigid bodies. *Phys. Fluids* **26**, 082001.

NELSON, B. J., KALIAKASTOS, I. K. & ABBOTT, J. J. 2010 Microrobots for minimally invasive medicine. *Ann. Rev. Biomed. Eng.* **12** (1), 041916.

PAVLICK, R. A., DEY, K. K., SIRJOOSINGH, A., BENESI, A. & SEN, A. 2013 A catalytically driven organometallic molecular motor. *Nanoscale* **5**, 1301–1304.

PAVLICK, R. A., SENGUPTA, S., MCFADDEN, T., ZHANG, H. & SEN, A. 2011 A polymerization powered-motor. *Angew. Chem. Intl Ed.* **50**, 9374–9377.

PAXTON, W. F., KISTLER, K. C., C.C., O., SEN, A., ANGELO, S. K. S., MALLOUK, Y., THOMAS, E., LAMMERT, P. E. & CRESPI, V. H. 2004 Catalytic nanomotors: autonomous movement of stripped nanorods. *J. Am. Chem. Soc.* **126** (41), 13424–13431.

PURCELL, E. M. 1977 Life at low Reynolds number. *Am. J. Phys.* **45**, 3–11.

QIAN, B., MONTIEL, D., BREGULLA, A., CICHOS, F. & YANG, H. 2013 Harnessing thermal fluctuations for purposeful activities: the manipulation of single microswimmers by adaptative photon nudging. *Chem. Sci.* **4**, 1420–1429.

RILEY, N. 1966 On a sphere oscillating in a viscous fluid. *Q. J. Mech. Appl. Maths* **XIX** (4), 461–472.

SABRINA, S., TASINKEVYCH, M., AHMED, S., BROOKS, A. M., OLVERA DE LA CRUZ, M., MALLOUK, T. E. & BISHOP, K. J. M. 2018 Shape-directed microspinners powered by ultrasound. *ACS Nano* **12** (3), 2939–2947.

SMOLUCHOWSKY, M. 1921 *Handbuch der Electrizitat und des Magnetismus*. Graetz (ed.), Leipzig.

STOKES, SIR G. G. 1850 On the effects of the internal friction of fluids on the motion of pendulums. *Trans. Camb. Phil. Soc.* **IX**, 8.

SUNDARARAJAN, S., LAMMERT, P. E., ZUDANS, A. W., CRESPI, V. H. & SEN, A. 2008 Catalytic motors for transport of colloidal cargo. *Nano Lett.* **8**, 1271–1276.

WANG, W., CASTRO, L. A., HOYOS, M. & MALLOUK, T. E. 2012 Autonomous motion of metallic microrods propelled by ultrasound. *ACS Nano* **6** (7), 6122–6132.

WANG, W., DUAN., W., AHMED, S., MALLOUK, T. E. & SEN, A. 2013 Small power: autonomous nano- and micromotors propelled by self-generated gradients. *Nano Today* **8**, 531–554.

WU, J., KAGAN, S. B. D., MANESH, K. M., CAMPUZANO, S. & WANG, J. 2010 Motion-based DNA detection using catalytic nanomotors. *Nat. Commun.* **1** (3), 36.

ZHANG, W. & STONE, H. A. 1998 Oscillatory motions of circular disks and nearly spherical particles in viscous flows. *J. Fluid Mech.* **367**, 329–358.